Wu, H., Böttger, R., Couffignal, F., Gutzmer, J., Krause, J., Munnik, F., Renno, A. D., Hübner, R., Wiedenbeck, M., Ziegenrücker, R. (2019): 'Box-Profile' Ion Implants as Geochemical Reference Materials for Electron Probe Microanalysis and Secondary Ion Mass Spectrometry. - *Geostandards and Geoanalytical Research*, *43*, 4, pp. 531—541.

DOI: http://doi.org/10.1111/ggr.12282

Vol. 43 — N° 4 12 19 p. 531 – 541

GEOSTANDARDS and GEOANALYTICAL RESEARCH

'Box-Profile' Ion Implants as Geochemical Reference Materials for Electron Probe Microanalysis and Secondary Ion Mass Spectrometry

Haosheng **Wu** (1), Roman **Böttger** (2), Frédéric **Couffignal** (3), Jens **Gutzmer** (1), Joachim **Krause** (1), Frans **Munnik** (2), Axel D. **Renno** (1), René **Hübner** (2), Michael **Wiedenbeck** (3) and René **Ziegenrücker** (2)

(1) Helmholtz Zentrum Dresden-Rossendorf (HZDR), Helmholtz Institute Freiberg for Resource Technology (HIF), Chemnitzer Str. 40, Freiberg, 09599, Germany
(2) Helmholtz Zentrum Dresden-Rossendorf (HZDR), Institute of Ion Beam Physics and Materials Research, Bautzner Landstrasse 400, Dresden, 01328, Germany
(3) Helmholtz Zentrum Potsdam, Deutsches GeoForschungsZentrum (GFZ), Telegrafenberg, Potsdam,14473,Germany
* Corresponding author. e-mail: haosheng.wu@hzdr.de

Although electron probe microanalysis and secondary ion mass spectrometry are widely used analytical techniques for geochemical and mineralogical applications, metrologically rigorous quantification remains a major challenge for these methods. Secondary ion mass spectrometry (SIMS) in particular is a matrix-sensitive method, and the use of matrix-matched reference materials (RMs) is essential to avoid significant analytical bias. A major problem is that the number of available RMs for SIMS is extremely small compared with the needs of analysts. One approach for the production of matrix-specific RMs is the use of high-energy ion implantation that introduces a known amount of a selected isotope into a material. We chose the more elaborate way of implanting a so-called 'box-profile' to generate a quasi-homogeneous concentration of the implanted isotope in three dimensions, which allows RMs not only to be used for ion beam analysis but also makes them suitable for EPMA. For proof of concept, we used the thoroughly studied mineralogically and chemically 'simple' SiO_2 system. We implanted either ^{47}Ti or ^{48}Ti into synthetic, ultra-high-purity silica glass. Several 'box-profiles' with mass fractions between 10 and 1000 μg g^{-1} Ti and maximum depths of homogeneous Ti distribution between 200 nm and 3 μm were produced at the Institute of Ion Beam Physics and Materials Research of Helmholtz-Zentrum Dresden-Rossendorf. Multiple implantation steps using varying ion energies and ion doses were simulated with Stopping and Range of Ions in Matter (SRIM) software, optimising for the target concentrations, implantation depths and technical limits of the implanter. We characterised several implant test samples having different concentrations and maximum implantation depths by means of SIMS and other analytical techniques. The results show that the implant samples are suitable for use as reference materials for SIMS measurements. The multi-energy ion implantation technique also appears to be a promising procedure for the production of EPMA-suitable reference materials.

Keywords: 'box-profile', multi-energy ion implantation, electron probe microanalysis, secondary ion mass spectrometry, synthetic reference material.

Received 15 Oct 18 – Accepted 19 May 19

Ion implantation allows the introduction of measurable amounts of almost any element into a wide range of different materials. With this possibility, ion implantation can be used to produce 'matrix-matched' reference materials for determination of trace elements by secondary ion mass spectrometry (SIMS). This approach is widely used in material science, and it has been shown to produce suitable calibrators for ion microprobe analyses in geoscience applications (Burnett *et al.* 2015), although it remains rarely used for geochemical applications. Examples of

doi: 10.1111/ggr.12282

geochemical applications are the quantification of phosphorus in crystalline quartz (Müller *et al.* 2008), determination of Li in melilite (Burnett *et al.* 2015), measurement of low atomic number elements in surface deposits of lunar soils (Zinner *et al.* 1976), quantification of carbon solubility in mantle minerals (Shcheka *et al.* 2006) and quantification of nitrogen solubility in upper mantle minerals (Yoshioka *et al.* 2018). In all of these applications, a single ion dose using a single kinetic energy was implanted into a substrate sample, in which case the implanted element in the bulk has a Gaussian-like depth distribution. Such inhomogeneity of the target element in implant-generated reference materials limits their use to only ion microprobe analyses performed with nanometre-scale depth resolution. Such reference materials are poorly suited for use in electron probe analyses.

In order to extend the use of implant-generated RMs to other analytical methods, here we investigate the suitability of multi-energy ion implantation. For proof of concept, we implanted high-purity silica glass with either ^{47}Ti or ^{48}Ti with quasi-homogeneous concentrations as a function of depth and with nominal mass fractions ranging from 10 to 1000 μg g^{-1}. As an important trace element in quartz, Ti^{4+} can substitute for tetrahedrally co-ordinated silicon (Müller *et al.* 2003). The amount of substitution reflects the *P-T* conditions at the time of quartz crystallisation, meaning that Ti mass fraction in quartz is suitable as a geothermobarometer. Based on the experimental study of Ti content over a range of pressure–temperature conditions, quartz that crystallises in most geological settings will have Ti contents in the range 1–100 μg g^{-1} (Wark and Watson 2006, Thomas *et al.* 2010). As the result of metamorphic recrystallisation of quartz, trace element mass fractions in natural quartz are commonly inhomogeneous across small spatial scales (Müller *et al.* 2003, Cherniak *et al.* 2007, Rusk *et al.* 2008, Lehmann *et al.* 2009). Consequently, using trace element mass fractions in low-temperature quartz for petrogenetic reconstructions requires techniques capable of detecting low elemental values (~ 1 μg g^{-1}) from small (< 25 μm^3) regions of solid samples, which can be achieved using the SIMS method.

A series of reference materials have already been produced and characterised for this application. A commonly used crystalline material is the TitaniQ series of high-Ti quartz grown by Thomas *et al.* (2010), which is a suite of single crystals containing 20, 100, 380 and 760 μg g^{-1} Ti. As TitaniQ series were produced according to equilibrium solubility, they are limited to those mass fractions attainable by experiments; this approach is unsuitable for addressing quartz that crystallised in low-temperature settings where Ti mass fractions below 10 mg g^{-1} can be expected.

The NIST SRM 610–617 glasses are widely used for calibrating trace element measurements; however, it must be noted that these glasses were not originally produced for use as reference materials for microanalysis (Kane 1998). Major element compositional differences between natural glass samples and NIST reference materials are likely to cause variations in ionisation yields that are not uniform between the different elements or isotopes of a given element. Due to this matrix effect, NIST SRM 610–617 are not suitable for the quantification of certain elements in quartz (Behr *et al.* 2011, Leeman *et al.* 2012, Cruz-Uribe *et al.* 2017).

Select natural quartz has been successfully tested for use as calibration materials for trace element determination (Audetat *et al.* 2015). Also, a set of four silica glasses with known contents of Ti were prepared at the University of Edinburgh (Gallagher and Bromiley 2013). Recently, multi-layered nanoporous silica gel was used to produce Ti-doped high-purity silica glass (Nachlas 2016). Although all these materials may be useful under some analytical conditions, their suitability as reference material is limited for microanalytical methods. On the other hand, the availability of these painstakingly prepared and studied reference materials allowed thoroughly chemical analyses of our samples.

From simulation to reality: multi-energy ion implantation

Ion implantation of Ti into SiO_2

As starting materials, we used Suprasil® 1 wafers, which are composed of high-purity synthetic silica glass. Suprasil® glass was produced by flame hydrolysis of $SiCl_4$ under strictly controlled conditions. They are bubble- and inclusion-free, with a bubble class better than 0 according to .

Ion implantation is a well-established technique. Commercially available ion implanters are capable to implant ions covering most of the periodic table of elements with concentrations ranging from 10^9 to 10^{18} atoms cm^{-3}, where the dose distribution can be precisely controlled through a combination of integrated ion current and impact energy of the species being implanted. Mean penetration depths ranging from 1 nm to 100 μm can be set very precisely by controlling the energy of the ions from 10 to 10^8 keV (Schmidt and Wetzig 2012). A further advantage of the ion implantation method is that specific isotopes can be selected which are the least affected by isobars or molecular ions

using an analytical magnet. Hence, there is a very wide diversity in the range of implant RMs that can be produced.

We modelled the theoretical depth distributions of titanium $R_{Ti}(x)$ (atoms cm^{-1}) in our Suprasil® target material using the software SRIM (Stopping and Ranges of Ions in Matter, Ziegler *et al.* 2008). This software uses a Monte Carlo code that calculates the interactions of energetic ions with an amorphous target. SRIM simulates ion trajectories using an approximation based on two-body collisions.

Implantation of Ti 'box-profiles'

We prepared our samples at the Institute of Ion Beam Physics and Materials Research of the Helmholtz-Zentrum Dresden-Rossendorf (HZDR) using three ion implanters, which had maximum accelerator voltages of 500, 200 and 40 kV, respectively. One consideration in our experimental design was the technically lowest achievable fluence of 10^{11} atoms cm^{-2} for the available 500 kV implanter, while both the 200 and 40 kV implanters were limited to 10^{12} atoms cm^{-2}. In order to assure a homogeneous titanium distribution in the silica glass end product, multi-implantation employs as many different implantation energies as reasonable while also taking the technical limitations into account. Hence, the implantation parameters for our 'box-profiles' were calculated so as to limit any deviation of the target concentration to < 5% across the entire depth of the profile (see Figure 1).

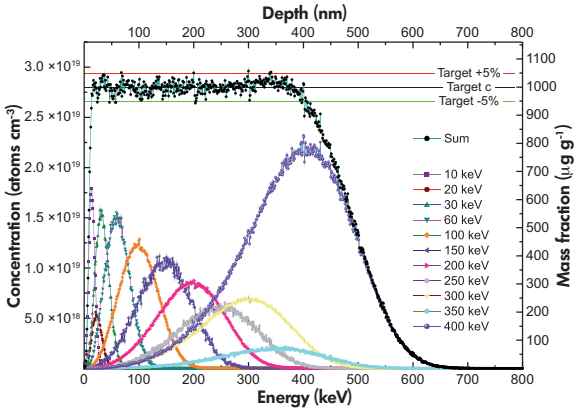

Figure 1. Simulation result of 1000 µg g^{-1} Ti distribution in silica glass from near surface (~ 10 nm) to 400 nm depth by summing optimised doses for different simulated depth profiles. Under this simulation, the sample HIFS_4 was produced. [Colour figure can be viewed at wileyonlinelibrary.com]

The common description of target concentration ξ (µg g^{-1}) can be converted with known matrix density ρ (g cm^{-3}), target element molar mass M (g mol^{-1}) and the Avogadro constant N_A (atom mol^{-1}) to the required ion concentration N (atom cm^{-3}) of the implant species. Hence, we calculated the Ti isotope concentration N_{Ti} (^{47}Ti or ^{48}Ti) for the required Ti mass ratio ξ_{Ti} with known silica glass density ρ_{SiO_2} (2.22 g cm^{-3}), Ti molar mass M_{Ti} and the Avogadro constant N_A from Equation :

$$N_{Ti} = \xi_{Ti} \cdot \frac{N_A}{M_{Ti}} \cdot \rho_{SiO_2} \quad (1)$$

By simulating the Ti depth profiles $R_{Ti}(x)$ (atoms cm^{-1}) using SRIM, the required amount of Ti isotope concentration (atoms cm^{-3}) can be calculated with the chosen fluence ϕ_{Ti} (atoms cm^{-2}), which can be calculated from the equation:

$$N_{Ti}(x) = \varphi_{Ti} \cdot R_{Ti}(x) \quad (2)$$

The Ti isotope concentration of a multi-energy ion implantation is the sum of each individual Ti isotope concentration, which can be represented as a function of x, the stopping range of Ti isotope ions.

$$N_{Ti}(x) = \sum \varphi_{Ti} \cdot R_{Ti}(x)_i \quad (3)$$

Based on Equation 3, fifteen samples were produced; the sample parameters are given in Table 1 (more information in Appendix 1).

Table 1.
Implant dose and implant depth of the chosen isotope of Ti in each sample

Sample	Implanted isotope	Mass fraction (µg g^{-1})	Depth (nm)
HIFS_1	^{48}Ti	100	200
HIFS_2	^{48}Ti	1000	300
HIFS_3	^{48}Ti	100	300
HIFS_4	^{48}Ti	1000	400
HIFS_5	^{48}Ti	100	400
HIFS_6	^{48}Ti	1000	200
HIFS_7	^{47}Ti	10	500
HIFS_8	^{47}Ti	100	500
HIFS_9	^{47}Ti	1000	500
HIFS_10	^{48}Ti	10	500
HIFS_11_1	^{48}Ti	100	500
HIFS_11_2	^{48}Ti	100	500
HIFS _11_3	^{48}Ti	100	500
HIFS_11_4	^{48}Ti	100	500
HIFS_11_5	^{48}Ti	100	500
HIFS_12	^{47}Ti	100	3000

Analytical techniques

Electron probe microanalysis

The Ti contents of five samples (HIFS_2, HIFS_5, HIFS_7, HIFS_9 and HIFS_12) were determined using a JEOL JXA-8530F electron probe microanalyser at the Helmholtz Institute Freiberg for Resource Technology (HIF), which was equipped with five wavelength-dispersive (WD) and one energy-dispersive (ED) spectrometer. Prior to electron probe microanalysis (EPMA) measurements, the samples were rinsed with ethanol and dried in a vacuum oven for 24 h followed by coating with a *ca.* 20-nm-thick high-purity carbon film; the samples were subsequently stored in a desiccator until the time of analysis.

As internal reference for quantitative analysis of Ti content, the intensity of the Si-K_α line was measured with a J-type PET spectrometer, while the intensity of the Ti K_α line was measured with an L-type PET, an L-type LIF, an H-type PET and an H-type LIF spectrometer. In order to constrain the analysis volume for Ti to within the implant depths, the acceleration voltages used for our sample were varied across 5, 10, 12.5, 15, 17.5, 20 and 25 kV. A current of 100 nA and a beam size of 10 μm were applied for all of the EPMA measurements. The counting time was set to 100 s on the peak and 25 s on both the high and low backgrounds. Rutile and diopside from Astimex Standards Ltd. (Toronto, ON, Canada) were used for calibration.

Particle-induced X-ray emission

The Ti contents of four samples (HIFS_1- HIFS_4) were measured with Particle-induced X-ray emission (PIXE). Two sets of PIXE measurements were performed at the Institute of Ion Beam Physics and Materials Research of HZDR using either an 850 keV or a 1.7 MeV proton beam. The implanted samples were fixed to the sample holder with copper foil tapes. To further minimise sample charging, an extra copper foil tape and a steel strand connecting the sample surfaces and the sample holder were attached to the sample. These also served to fix the samples on the holder, which was a concern as the sample holder had a vertical orientation in the chamber during the experiments.

The software *Gupixwin* (Campbell *et al.* 2010) was used to extract peak intensities and convert these to concentration values via the fixed-matrix solution method. A two-layer sample model was used for the analysis: the first layer being the gold coat and the second the implant layer of the underlying glass.

Secondary ion mass spectrometry

The Ti contents and Ti depth profiles of all samples were measured independently using two types of secondary ion mass spectrometers: a Cameca IMS 7f-Auto at the HZDR HIF laboratory and a Cameca IMS 1280-HR at Helmholtz Centre Potsdam-German Research Centre for Geosciences (GFZ). Prior to SIMS measurements, the samples were ultrasonically cleaned for 5 min in high-purity ethanol, dried and were coated with a *ca.* 35 nm thick high-purity conductive Au film.

At GFZ, a 13 keV $^{16}O^-$ primary ion beam was used in conjunction with +10 kV as applied to the sample holder in the secondary ion source, resulting in a total impact energy of 23 keV. Of the five stable Ti isotopes, we implanted either the major isotope ^{48}Ti (73.74% natural abundance) or ^{47}Ti (7.44%); the interferences affecting both isotopes can be separated with mass resolution ($M/\Delta M$) higher than ~ 2000 (Behr *et al.* 2011). However, for higher precision of the isotope signal, the interference $^{16}O_3^+$ seems to not be completely avoided at $M/\Delta M \approx 2000$. Thus, we took advantage of the large geometry of the Cameca IMS 1280-HR to use $M/\Delta M \approx 4000$. For the Cameca IMS 1280-HR, we used exclusively the EM in the mono-collection detector system. A single measurement cycle consisted of peak-stepping sequence from $^{30}Si^+$ (1 s integration time) to $^{48}Ti^+$ (4 s) or $^{47}Ti^+$ (4 s). The total analysis times were adjusted to assure that our profiles reach the bottom of the implant zone. In order to maintain sufficient secondary ion intensities, a $M/\Delta M \approx 2000$ was used for the IMS 7f-Auto depth profiles. For the profiles run on the small geometry instrument both the ^{28}Si and ^{30}Si were used as internal reference, the dominant isotope ^{28}Si was detected using the FC while $^{30}Si^+$ and $^{47}Ti^+$ or $^{48}Ti^+$ were detected using the EM. Two types of measurement recipes were applied. One consisted of the peak-stepping sequence from $^{30}Si^+$ (3 s integration time) and either $^{47}Ti^+$ (10 s) or $^{48}Ti^+$ (10 s). The other consisted of the peak-stepping sequence from $^{28}Si^+$ (3 s) and either $^{47}Ti^+$ (10 s) or $^{48}Ti^+$ (10 s). More important parameters of SIMS depth profiling measurement are shown in Table 2. These settings assured that only ions originating from the flat bottom portion of the crater would reach the respective ion detection system (see Figure 2). Furthermore, the raw count rate for Si and Ti also indicate that there was no charging effect, also signals from the crater walls were not detected (see Figures S1 and S2 in Appendix S2).

We used a set of four silica glasses from the University of Edinburgh as reference materials (Gallagher and Bromiley 2013). Bubbles in these samples, which are difficult to avoid due to the production process, were seen to affect the

Table 2.
Important parameters for depth profiling measurements with the IMS 1280-HR and IMS 7f-Auto instruments

Parameter	IMS 1280-HR	IMS 7f-Auto
Primary ions	O^-	O^-
Primary current	23 nA	18 nA
Primary beam size	~ 10 µm	~ 35 µm
Source extraction voltage	-13 kV	-13 kV
Incident angle	23.6°	23.6°
Impact energy	23 keV	21 keV
Energy band pass	150 eV	69 eV
Mass resolution (M/ΔM) at 10%	4000	2000
Raster size	70 × 70 µm	Ø 250 µm
Analysed area	10 × 10 µm	Ø 100 µm
Pre-sputtering time	20 s	300 s
Cycles	399	800

measured data despite our best efforts to avoid them. However, this influence can be minimised by careful selection of measurement points.

Transmission electron microscopy

So as to understand better the microstructure and element distributions within the implanted layer and the non-implanted substrate, transmission electron microscopy (TEM) analyses were performed on one of our samples. For this purpose, classical TEM cross sections of sample HIFS_5 glued together in face-to-face geometry were prepared by sawing, grinding, polishing, dimpling and final Ar ion milling. Prior to TEM analysis, the specimen, mounted in a high-visibility low-background holder, was cleaned for 10 s with a Model 1020 Plasma Cleaner (Fischione, Hanau, Germany).

Both high-resolution TEM imaging and spectrum imaging based on energy-dispersive X-ray spectroscopy (EDXS) were conducted with 200 keV electrons using a Talos F200X microscope equipped with an X-FEG electron source and a Super-X EDXS detector system (FEI).

Results and discussion

Electron probe microanalysis

Because the original sample production strategy focussed on SIMS calibration, Ti contents were kept generally low and the implant depth for the length of the 'box-profiles' was targeted for at most 3 µm. These are not ideal parameters for electron probe analyses, and hence the aim of the EPMA measurement was to estimate the feasibility of using multi-energy ion implantation as a production procedure for EPMA-suitable RMs and also to define the optimal setup with relation to implantation depth and concentration of implanted ions.

As Ti L emission lines (0.585 keV for L_I, 0.460 keV for L_{II} and 0.454 keV for L_{III}) are low energy lines with low ionisation cross sections, no Ti L lines were detected despite varying the acceleration voltage from 5 to 25 kV. We

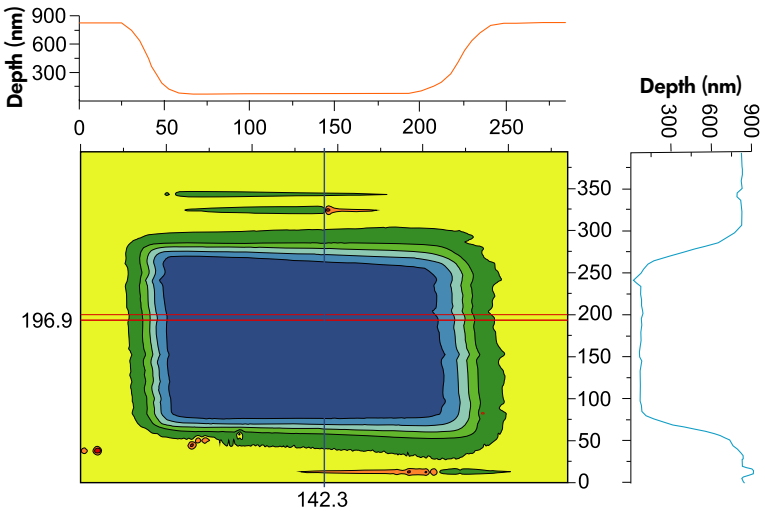

Figure 2. 2D image of one IMS 7f-Auto sputtered crater on the implant sample HIFS_4 measured by stylus profilometry with depth information of the bottom. [Colour figure can be viewed at wileyonlinelibrary.com]

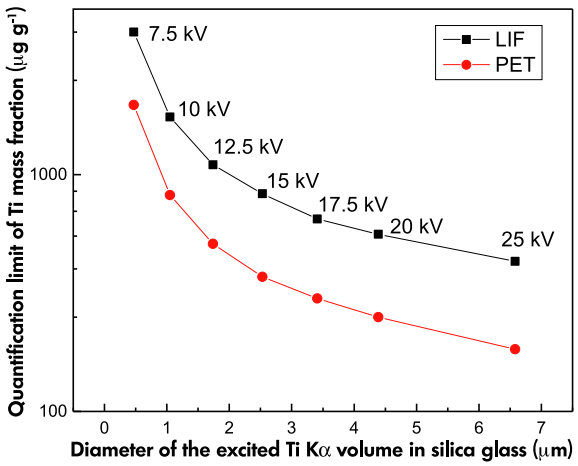

Figure 3. Quantification limit of Ti mass fraction as a function of depth of the excited Ti Kα X-ray in silica glass by EPMA measurement using WD spectrometers with PET and LIF. Quantification limit of Ti Kα lines were corrected with ZAF, PENEPMA Monte Carlo (Llovet and Salvat 2016) simulations were used to simulate the diameter of the excited Ti Kα volume under different acceleration voltages. [Colour figure can be viewed at wileyonlinelibrary.com]

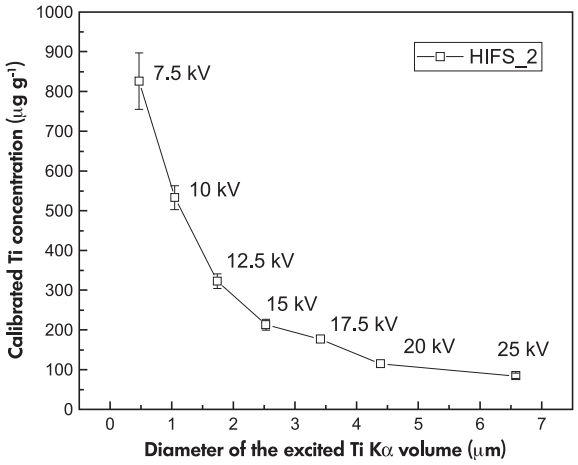

Figure 4. Calibrated Ti contents of HIFS_2 as function of diameter of the excited Ti Kα volume with various acceleration voltage from 7.5 to 25 kV. Content values were calculated from L-type PET results corrected with ZAF; uncertainty is standard deviation (1*s*). Diameter of the excited Ti Kα volume was simulated using PENEPMA (Llovet and Salvat 2016). As intensities measured with higher acceleration voltage have smaller relative standard deviation, the measured points starting from 17.5 kV cover their error bars.

conclude that the ideal strategy for quantification in this case is to use the Ti Kα line. Results measured using a H-type PET crystal caused a large measurement bias because the lower side of the peaks could not be measured, whereas L-type PET provided peak to background ratio, which was better by more than a factor of two. Nevertheless, a Ti content of 100 µg g^{-1} remains close to the limit of detection for EPMA (Llovet and Salvat 2016) using an L-type PET detector crystal. An acceleration voltage ≥ 17.5 kV should generate a sufficient TiKα count rate, which comes from a depth of at least 3.4 µm within a silica glass sample (Figure 3, simulated using PENEPMA). The calibrated Ti content of HIFS_12, which contains 100 µg g^{-1} Ti within an implant layer thickness of approximately 3 µm, is thus marked by a high standard deviation (1*s*): 89 ± 24.3 µg g^{-1} (L-type LIF), 104 ± 10.5 µg g^{-1} (L-type PET).

As all the samples containing 1000 µg g^{-1} Ti have shallow implant layers (shorter than 500 nm), a clear decrease in the apparent Ti content was observed with increasing acceleration voltage (Figure 4).

Particle-induced X-ray emission

Low mass fractions of Cr and Fe were detected with PIXE. These are assumed to be associated with the gold coating. In the 1.7 MeV measurements, Cu was found. It is considered a parasitic element coming from the Cu tape used in the sample holder.

Two proton beam energies were used: 850 keV and 1.7 MeV. The use of the lower proton energy yielded a lower Bremsstrahlung background. Since the Ti signal for samples HIFS_1 and HIFS_3 was below the detection limit, the second suite of analyses used a higher proton energy so as to increase the cross section for ionisation of the Ti K-shell with the goal of achieve a better peak to background ratio. However, in both cases the detection limit remained relatively high. Ultimately Ti could only be quantified with PIXE in the implanted sample that contained 1000 µg g^{-1} (see Figure 5, Table 3 and Appendix S3). Based on the measurement result, the 1000 µg g^{-1} implanted samples reported the expected implant concentration with analytical uncertainties within ± 5%.

Secondary ion mass spectrometry

The normalised Ti isotopes signals of the implanted samples were initially analysed as depth profiles in order to evaluate homogeneity of the Ti distribution in three dimensions. Subsequently, quantitative determinations of Ti

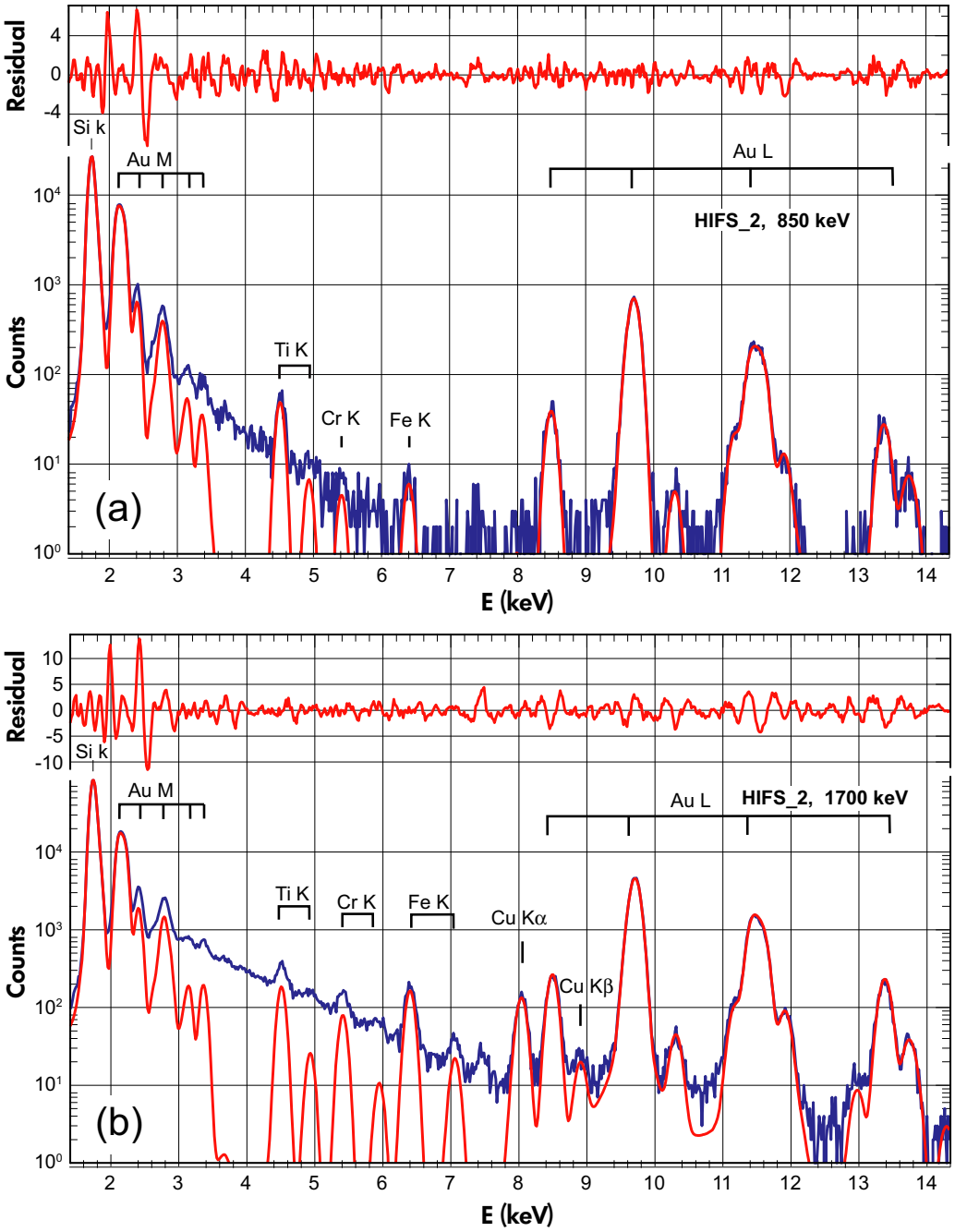

Figure 5. ***Gupixwin*-fitted graph of PIXE spectra of HIFS_2 using (a) 850 keV proton energy and (b) 1700 keV proton energy. PIXE spectra provide the intensity of the characteristic X-rays and Bremsstrahlung background as a function of the X-ray energy. The red curve of the PIXE spectrum illustrates the intensities of characteristic X-rays of the determined elements obtained from the *Gupixwin* fit. The residual shows the difference between data and fit with background taken into account. [Colour figure can be viewed at wileyonlinelibrary.com]**

concentration as a function of depth were conducted using calibrations derived from the silica glass-derived materials provided by the University of Edinburgh (Gallagher and Bromiley 2013). Furthermore, in order to test the reproducibility of our implantation process, depth profiles of a series of implanted samples having the same 'box-profile' were compared and the Ti concentrations were quantitatively determined.

Table 3.
Weighted means and their respective standard deviations of sample HIFS_2 and HIFS_4 (implanted Ti mass fraction of 1000 μg g^{-1}) analysed using the PIXE measurements

Sample	Mean (μg g^{-1})	1*s* (μg g^{-1})
HIFS_2	1043	54.2
HIFS_4	930	40.2

Values calculated by Haosheng Wu.

Depth profiles

The SIMS depth profiles that we measured closely matched the Monte Carlo simulation (see Figure 6). Including the SIMS measurement uncertainty, the observed lateral deviation (2*s*) in Ti contents was 2.8% and the deviation (2*s*) of Ti content across the implant depth was 4.8%.

The five implanted samples generated for the reproducibility test (HIFS_11_1, HIFS_11_2, HIFS _11_3, HIFS_11_4 and HIFS_11_5) were implanted with nominal abundances of 100 μg g^{-1} Ti at depths ranging from 60 to 500 nm (Table 4). Each sample was measured four times using spatially dispersed measuring points. Their SIMS depth profiles show good repeatability. Based on twenty SIMS analyses, the variability of lateral Ti contents was < 5% (Figure 7).

Published single-energy ion implantation results (Burnett *et al.* 2015) have reported inaccuracies in the nominal implant fluence reaching up to ~ 30%. As compared with single-energy ion implantation profile, an important advantage of multi-energy ion implantation is the ability to check the accuracy of implant contents directly through SIMS depth profiling. By repeating the same implant fluence (ions cm^{-2}) within a specified depth range, a 'box-profile' is capable of testing the precision of the implantation by assessing its near-surface evenness. We observed slightly higher count rates of implanted Ti from shallow implant side for all the samples implanted with 1000 μg g^{-1} Ti. For the samples targeting a 1000 μg g^{-1} Ti mass fraction, each Ti implant with fluence

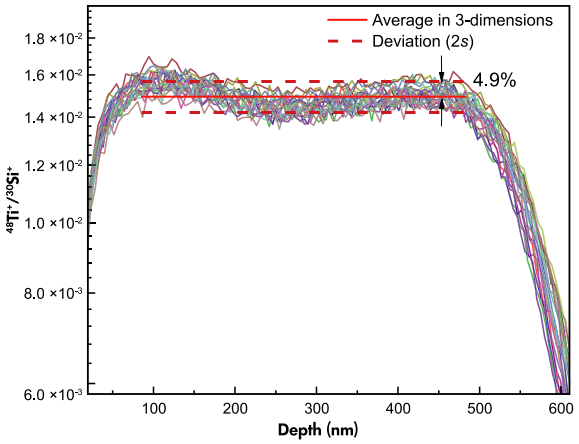

Figure 7. $^{48}Ti^+/^{30}Si^+$ ratio intensities of twenty measurement points in all HIFS_11 samples (HIFS11_1 to HIFS11_5, 4 points for each sample) as a function of depth. [Colour figure can be viewed at wileyonlinelibrary.com]

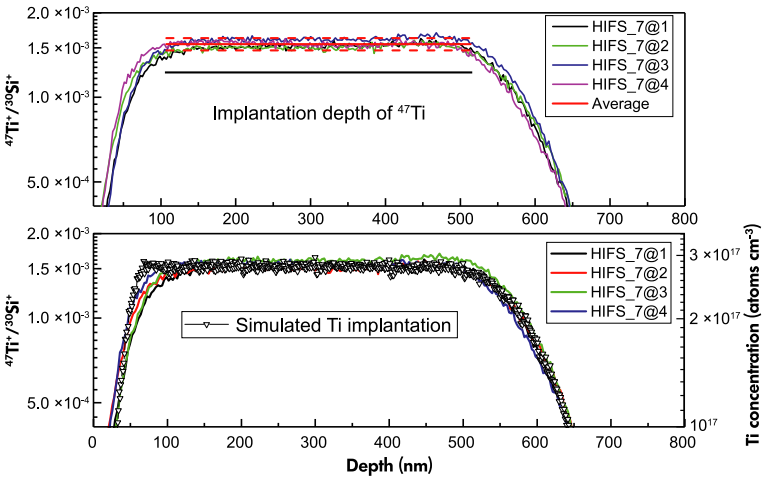

Figure 6. Ratio of the $^{47}Ti^+/^{30}Si^+$ intensities as a function of depth in HIFS_7 applying optimised doses at different energies, the first 35 nm is the gold coating; the black solid line shows the aimed implantation depth. Average is the average in three dimensions of four measurement points within the implantation depth with dotted line showing the 95.45% confidence interval. The line with inverted triangle shows the simulate Ti distribution in the silica glass sample simulated by SRIM. [Colour figure can be viewed at wileyonlinelibrary.com]

Table 4.
Ion energy and implant doses for 100 μg g^{-1} Ti in silicate glass from 60 nm to 500 nm

Energy (keV)	60	100	150	200	250	300	350	400	500
Fluence (atom cm^{-2}) × 10^{13}	0.85	1.10	1.30	1.30	1.00	1.90	1.00	0.90	7.00

Values simulated by Haosheng Wu.

combination ranged from 8 × 10^{13} to 9 × 10^{14} atom cm^{-2} seems to be difficult to reproduce in practice. For further discussion, refer to Appendix S2.

Ti mass fraction

For determination of Ti mass fraction in a silica matrix, the data from the depth profiling measurement from both IMS 1280 and IMS 7f-Auto instruments were used. The following equation (4) was used:

$$\left[\frac{\frac{^{47}Ti^{+}}{^{30}Si^{+}}}{\frac{(^{47}Ti)\ \text{atom ppm}}{(Si)\ \text{atom}\ \%}}\right]_{RM} = \left[\frac{\frac{^{47}Ti^{+}}{^{30}Si^{+}}}{\frac{(Ti)\ \text{atom ppm}\cdot f^{47}Ti}{(Si)_{\text{atom}\%}}}\right]_{\text{implant}} \quad (4)$$

The right side of the equation is known. Furthermore, it can be assumed that this ratio, known as the relative sensitivity factor (RSF), is constant for a given combination of two elements for a given matrix under stable analytical conditions. To establish the RSF, the Ti mass fractions of silica glass-derived RMs were determined using both EPMA and ICP-OES (Gallagher and Bromiley 2013), along with the known molar concentration of Si in quartz (33.3%) and the measured count rate of ^{47}Ti and ^{30}Si. The mass ratios of ^{47}Ti in RMs were corrected with its natural abundances 7.44 atom%. Figure 6 illustrates how the intensity ratio of $^{47}Ti/^{30}Si^{+}$ from the implant profile was determined.

For the five implanted samples designed for the reproducibility test of our implant method, an absolute Ti mass fraction of 116 μg g^{-1} with 13% uncertainty (1s) was determined when our data were calibrated using the silica glass RMs. For the other implanted samples, the measured Ti mass fractions are in good agreement with the simulated values (see Figure 8). Since there was systematic bias during the production of 1000 μg g^{-1} Ti implants (Appendix S2), the high-Ti content group contains more uncertainty than the other samples.

Transmission electron microscopy

According to Figure 9, our Ti implantation did not lead to any significant microstructural changes; no differences

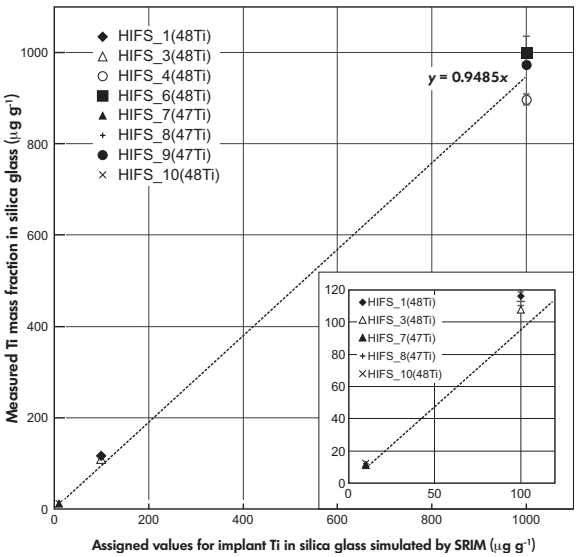

Figure 8. Measured Ti mass fraction in HIFS samples using silica gel-derived materials from Edinburgh (Gallagher and Bromiley 2013) as reference materials, error bars are the 95.45% confidence intervals of the means comparing with the assigned values for implant Ti in silica glasses using simulation software SRIM.

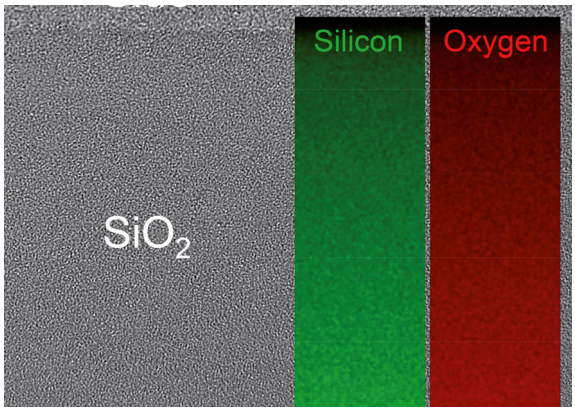

Figure 9. Cross-sectional high-resolution TEM image of sample HIFS_5 together with the Si and O element distributions obtained by energy-dispersive X-ray spectroscopy in scanning TEM mode. [Colour figure can be viewed at wileyonlinelibrary.com]

were found between the implanted and non-implanted sample regions. Rather, the silica glass remained amorphous without any signs for Ti-based exsolution of, for example metallic Ti or TiO_2 inclusions. Element mapping based on energy-dispersive X-ray spectroscopy confirmed the latter finding. Since the Ti content for all minor elements is below the detection limit of TEM, only the homogeneous Si and O element distributions are shown in the inset of Figure 9.

Conclusions

A range of 'box-profile' implants of Ti in amorphous silica was successfully produced, and these materials were assessed for their suitability as reference materials for ion probe microanalyses. TEM observations revealed no ion implantation-induced heterogeneity; the silica glass remained amorphous without any signs of Ti exsolution even at the nanometre scale. The SIMS depth profile measurements demonstrated that the homogeneity of Ti distribution within 'box-profile' was within our target uncertainty of ± 5%. The absolute Ti contents of our implanted materials were quantitatively measured by SIMS, PIXE and EPMA; these measurements show good agreement between the target implant doses and the observed Ti mass fractions. In the case of Ti implantation in silica glass, an implant depth of 3 μm with 1000 μg g^{-1} Ti shows already high measurement accuracy for EPMA. The multi-energy ion implantation technique thus seems very well suited to the production of a special type of geochemical reference material that can be used for trace element measurement by both SIMS and EPMA. In principle, all elements from hydrogen to uranium can be implanted individually, and there are no restrictions regarding the matrices. The maximal depth of the box-profiles is matrix dependent, but depths of ~ 5 μm can be achieved by using high-energy implantation set-ups.

Acknowledgements

We thank Romy Aniol, Bernd Scheumann and Sabine Gilbricht for technical assistance. Parts of this research were carried out at HZDR Ion Beam Centre. We would like to thank Dr. Johannes von Borany, Stefan Eisenwinder, Frank Ludewig, Franziska Nierobisch and Tobias Putzke for assistance. We are also indebted to Dr. John Craven for providing us the silica glass-derived materials from the University of Edinburgh. Furthermore, the use of HZDR Ion Beam Centre TEM facilities and the funding of TEM Talos by the German Federal Ministry of Education of Research (BMBF), Grant No. 03SF0451 in the framework of HEMCP are acknowledged.

References

Audetat A., Garbe-Schönberg D., Kronz A., Pettke T., Rusk B., Donovan J.J. and Lowers H.A. (2015)
Characterisation of a natural quartz crystal as a reference material for microanalytical fetermination of Ti, Al, Li, Fe, Mn, Ga and Ge. Geostandards and Geoanalytical Research, 39, 171–184.

Behr W.M., Thomas J.B. and Hervig R.L. (2011)
Calibrating Ti concentrations in quartz for SIMS determinations using NIST silicate glasses and application to the TitaniQ geothermobarometer. American Mineralogist, 96, 1100–1106.

Burnett D.S., Jurewicz A.J.G., Woolum D.S., Wang J., Paque J.M., Nittler L.R., McKeegan K.D., Humayun M., Hervig R., Heber V.S. and Guan Y. (2015)
Ion implants as matrix-appropriate calibrators for geochemical ion probe analyses. Geostandards and Geoanalytical Research, 39, 265–276.

Campbell J.L., Boyd N.I., Grassi N., Bonnick P. and Maxwell J.A. (2010)
The Guelph PIXE software package IV. Nuclear Instruments and Methods in Physics Research, Section B, 268, 3356–3363.

Cherniak D.J., Watson E.B. and Wark D.A. (2007)
Ti diffusion in quartz. Chemical Geology, 236, 65–74.

Cruz-Uribe A.M., Mertz-Kraus R., Zack T., Feineman M.D., Woods G. and Jacob D.E. (2017)
A new LA-ICP-MS method for Ti in quartz: Implications and application to high pressure rutile-quartz veins from the Czech Erzgebirge. Geostandards and Geoanalytical Research, 41, 29–40.

DIN 58927:1970-02.
Optisches Glas; Technische Lieferbedingungen. Beuth Verlag (Berlin).

Gallagher C. and Bromiley G. (2013)
Ti in quartz standards. https://www.ed.ac.uk/geosciences/facilities/ionprobe/standard-materials-available/tiquartzstandards

Kane J.S. (1998)
A history of the development and certification of NIST glass SRMs 610–617. Geostandards Newsletter: The Journal of Geostandards and Geoanalysis, 22, 7–13.

Leeman W.P., MacRae C.M., Wilson N.C., Torpy A., Lee C.T., Student J.J., Thomas J.B. and Vicenzi E.P. (2012)
A study of cathodoluminescence and trace element compositional zoning in natural quartz from volcanic rocks: Mapping titanium content in quartz. Microscopy Microanalysis, 18, 1322–1341.

Lehmann K., Berger A., Götte T., Ramseyer K. and Wiedenbeck M. (2009)
Growth related zonations in authigenic and hydrothermal quartz characterized by SIMS-, EPMA-, SEM-CL- and SEM-CC-imaging. Mineralogical Magazine, 73, 633–643.

references

Llovet X. and Salvat F. (2016)
PENEPMA: A Monte Carlo programme for the simulation of X-ray emission in EPMA. **IOP Conference Series: Materials Science and Engineering**, **109**, 012009.

Müller A., Wiedenbeck M., van den Kerkhof A.M., Kronz A. and Simon K. (2003)
Trace elements in quartz – A combined electron microprobe, secondary ion mass spectrometry, laser-ablation ICP-MS, and cathodoluminescence study. **European Journal of Mineralogy**, **15**, 747–763.

Müller A., Wiedenbeck M., Flem B. and Schiellerup H. (2008)
Refinement of phosphorus determination in quartz by LA-ICP-MS through defining new reference material values. **Geostandards and Geoanalytical Research**, **32**, 361–376.

Nachlas W.O. (2016)
Precise and accurate doping of nanoporous silica gel for the synthesis of trace element microanalytical reference materials. **Geostandards and Geoanalytical Research**, **40**, 505–516.

Rusk B.G., Lowers H.A. and Reed M.H. (2008)
Trace elements in hydrothermal quartz: Relationships to cathodoluminescent textures and insights into vein formation. **Geology**, **36**, 547–550.

Schmidt B. and Wetzig K. (2012).
Ion beams in materials processing and analysis. **Springer** (Wien).

Shcheka S.S., Wiedenbeck M., Frost D.J. and Keppler H. (2006)
Carbon solubility in mantle minerals. **Earth and Planetary Science Letters**, **245**, 730–742.

Thomas J.B., Watson E.B., Spear F.S., Shemella P.T., Nayak S.K. and Lanzirotti A. (2010)
TitaniQ under pressure: The effect of pressure and temperature on the solubility of Ti in quartz. **Contributions to Mineralogy and Petrology**, **160**, 743–759.

Wark D.A. and Watson E.B. (2006)
TitaniQ: A titanium-in-quartz geothermometer. **Contributions to Mineralogy and Petrology**, **152**, 743–754.

Yoshioka T., Wiedenbeck M., Shcheka S. and Keppler H. (2018)
Nitrogen solubility in the deep mantle and the origin of Earth's primordial nitrogen budget. **Earth and Planetary Science Letters**, **488**, 134–143.

Ziegler J.F., Biersack J.P. and Ziegler M.D. (2008).
SRIM, the stopping and range of ions in matter. **SRIM Company** (Chester).

Zinner E., Walker R., Chaumont J., Dran J. and Zinner E. (1976)
Ion probe analysis of artificially implanted ions in terrestrial samples and surface enhanced ions in lunar sample 76215,77. **7th Lunar Science Conference**, 953–984.

Supporting information

The following supporting information may be found in the online version of this article:

Appendix S1. Ion implantation.

Appendix S2. Secondary ion mass spectrometry.

Appendix S3. PIXE measurement.

This material is available from: http://onlinelibrary.wiley.com/doi/10.1111/ggr.12282/abstract (This link will take you to the article abstract).